Plasma Sources Science and Technology

Calculated electron impact dissociation cross sections for molecular chlorine (Cl$_2$)

To cite this article: James R Hamilton *et al* 2018 *Plasma Sources Sci. Technol.* **27** 095008

View the article online for updates and enhancements.

IOP ebooks™

Bringing you innovative digital publishing with leading voices to create your essential collection of books in STEM research.

Start exploring the collection - download the first chapter of every title for free.

Calculated electron impact dissociation cross sections for molecular chlorine (Cl₂)

James R Hamilton[1], Jonathan Tennyson[1], Jean-Paul Booth[2], Timo Gans[3] and Andrew R Gibson[2,3,4]

[1] Department of Physics and Astronomy, University College, London, Gower St., London WC1E 6BT, United Kingdom
[2] LPP, CNRS, Ecole Polytechnique, UPMC Univ. Paris 06, Univ. Paris-Sud, Université Paris-Saclay, Sorbonne Universités, F-91128 Palaiseau, France
[3] York Plasma Institute, Department of Physics, University of York, Heslington, York, YO10 5DD, United Kingdom

E-mail: j.tennyson@ucl.ac.uk and andrew.gibson@york.ac.uk

Abstract

Electron impact dissociation of Cl_2 is a key process for the formation of Cl atoms in low-temperature plasmas used for industrial etching processes. Despite this, relatively little cross section data exist for this process. In this work, electron impact dissociation cross sections were calculated for Cl_2 molecules using the UK molecular **R**-matrix code in the low electron energy range and extended to high energies using a scaling depending on the specific nature of each transition. Our results are compared with both previous calculations and with experimental measurements, and the similarities and differences are discussed. In addition, the rate coefficients for electron impact dissociation of Cl_2 are calculated by integrating the cross sections derived in this (and previous) work, with electron energy distribution functions representative of those normally found in low-temperature plasmas used in industry. Depending on the shape and effective temperature of the distribution function, significant differences arise between the rate coefficients calculated from our cross sections and those calculated using previous data. Deviations between the two sets of rate coefficients are particularly pronounced at the low electron temperatures typical of electron beam and remote plasma sources of interest for atomic layer etching and deposition. These differences are principally caused by the higher energy resolution in the near-threshold region in this work, emphasising the importance of accurate, high-resolution cross sections in this energy range.

Keywords: chlorine, cross sections, *r*-matrix, atomic layer etching, plasma modelling

1. Introduction

Chlorine plasmas are commonly used for etching processes in the semiconductor industry [1–3]. In these applications, the concentration of chlorine atoms (Cl) and ions (Cl_2^+, Cl^+, and Cl^-), principally produced from chlorine molecules (Cl_2) by

electron impact, are key parameters in determining process outcomes. In this context, accurate electron impact dissociation cross sections are essential for understanding chlorine atom production in these systems, and for use in simulation-based process design. In addition, electron impact excitation cross sections, whether dissociative or not, are necessary for the construction of the cross section sets needed as inputs to plasma models for the calculation of electron energy distributions and transport parameters [4, 5]. Due to the highly corrosive and toxic nature of Cl_2, experimental measurements of its cross-sections require specialised safety measures and often costly experimental systems. In this context, recent advances in theoretical calculations of such cross sections

---

[4] The author to whom any correspondence should be addressed

make them an attractive, safe and relatively cost-effective alternative to experimental measurements.

The Cl_2 molecule is also interesting from a theoretical perspective as it exemplifies important phenomena associated with electron interactions with simple molecules while having potential energy curves that are relatively straightforward to interpret. Thus, electron collisions with Cl_2 provide a good test system for theoretical models, allowing algorithmic frameworks to be established in conjunction with a conceptual interpretation of the potential energy curves. These frameworks can then be applied to the study of more complex polyatomic molecules where interpretation of potential energy surfaces is non-trivial.

Electron impact cross sections for Cl_2 have previously been reviewed by Christophorou and Olthoff [6] and more recently by Gregório and Pitchford [7]. Based on these reviews and an independent literature search it is clear that electron impact cross section data, and electron swarm parameter measurements, for Cl_2 are more limited than those for other diatomic molecules such as O_2 and N_2, which are easier to use experimentally. In particular, direct determinations of the cross sections for electron impact vibrational excitation [8, 9] and electronic excitation/dissociation [10–12] are rare. The only previous calculations of electronic excitation cross sections for Cl_2, focussed on dissociation to two neutral atoms, were carried out by Rescigno [10]. The recent work of Yadav *et al* [13] presents calculated electron impact excitation cross sections, without specifically considering whether or not dissociation to two neutral atoms occurs, for the first five excited states of chlorine, along with the total excitation cross section. Rescigno calculated state resolved dissociation cross sections corresponding to excitation into the first five lowest energy excited states of Cl_2, which were identified to dissociate into two Cl atoms. These calculations showed good agreement with the experimentally measured total dissociation cross section of Cosby [11, 12]. However, the calculations of Rescigno [10] have limited electron energy resolution, particularly close to the threshold energy of the excitation process, and are calculated up to a maximum energy of only 30 eV. Due to the relatively low electron temperatures encountered in industrial plasmas (in the range 0.3 – 5 eV) accurate, high-resolution cross sections in the threshold region of these processes are particularly important. The experimental data of Cosby [11, 12] on the other hand does not resolve the different excited states contributing to dissociation, and in addition, represents a sum of dissociation cross sections from multiple vibrational states of the ground electronic state [12]. However, the data of Cosby [12] does provide cross sections up to a higher energy of 100 eV.

In order to extend the available data for Cl_2 dissociation cross sections, and complement previous work in this area, we present new calculations for state-resolved electron-impact excitation cross sections for the electronic and ground state of Cl_2 over a wide energy range. Section 2 describes the processes and theoretical methods used in the calculations, section 3 describes the details of the calculations with respect to the target structure and the nature of the excited states, and section 4 presents the electron impact cross sections resulting

from our calculations, as well as rate coefficients calculated assuming different electron energy distributions.

2. Processes and theoretical methods

2.1. The ab initio R-matrix Method

The **R**-matrix method treats electron scattering from molecules by dividing the space of the problem into two separately-calculated regions [14], comprising an inner region containing the wavefunction of the molecular target along with the colliding electron, and an outer region in which only the incident, scattering electron is considered. The **R**-matrix calculation constructs and solves an electron-energy-independent wave equation for the inner region, whose solutions are then used to solve the much simpler, energy-dependent problem of the scattering electron in the outer region. By making the inner region of the problem independent of the colliding electron energy and only the outer region energy dependent, the outer region can be resolved on a very fine energy grid, showing all of the features and structure of the cross section.

The low-energy calculations reported in this work were all performed using the polyatomic implementation of the UK molecular **R**-matrix code UKRMol [15]. These calculations were performed using the Quantemol-N expert system [16] which runs the UKRMol codes. A full review of the molecular **R**-matrix method has been given in [17].

2.2. CAS-CI calculation model

Established electron scattering theory provides a range of models for treating the interaction of the incident scattering electron with the bound molecular electrons as discussed by Tennyson [17] and the references therein. In the scattering calculations carried out here, the selected target states were included in the scattering wavefunction through the use of a close-coupling (CC) expansion. Here, the target states are represented using a complete active space (CAS) configuration interaction (CI) model [18] in which bound electrons from the highest (valence) occupied molecular orbitals (HOMOs) are excited to the lowest unoccupied molecular orbitals (LUMOs). This model can calculate cross sections for electronically inelastic processes while also accounting reliably for Feshbach resonances, which are temporary anion states in which the scattering electron is trapped following excitation of the target.

2.3. Electron impact dissociation

Dissociation occurs when molecules are excited to electronic states that are either unbound or have curve-crossings to unbound states. The total electron impact dissociation cross section can therefore be taken to be the sum of excitation cross sections to all unbound states:

$$\sigma_{\text{eid}}^{\text{tot}} = \sum_{i=1}^{\infty} \sigma_{\text{ex}}^i , \qquad (1)$$

where $\sigma_{\mathrm{eid}}^{\mathrm{tot}}$ is the total electron impact dissociation cross section and σ_{ex}^{i} is the electron impact excitation cross section to a specific unbound state i. To fully understand the dynamics of electrons in low-temperature plasmas, electron-impact dissociation cross-sections via specific excited states, with specific excitation energies, i.e. σ_{ex}^{i}, should be known. In addition, it is important to know whether or not the atoms created by dissociation are created in excited states or the ground state, i.e. the branching ratio of the products. In this work, the nature of the orbitals populated by excitation collisions were used to ascertain whether or not an excitation process results in dissociation. The asymptotes of the potential energy curves for the dissociative excited states were used to determine the branching ratios of the dissociation products.

2.4. Extension of cross sections to high energies

The **R**-matrix model is known to provide accurate cross section data in the low energy range, defined here as between 0 eV and the ionisation potential (IP). For higher energies, the inelastic cross sections in this work are scaled according to the specific nature of the transition. In the case of dipole-forbidden transitions, i.e. those that involve a spin change, the cross section is scaled as $\frac{1}{\varepsilon}$, where ε is electron energy. In the case of dipole-allowed transitions, that is those with no spin change, the cross sections are scaled as $\frac{\ln(\epsilon)}{\epsilon}$. Where the calculated cross-sections showed non-physical structure at energies above the IP, this non-physical structure was assumed to be an artefact of the calculation, and smoothed. Such non-physical structure can arise in the calculations due to using only single geometry, incomplete continuum orbital sets, or due to pseudo-resonances. This method of scaling has previously been employed in [19].

3. Calculation details

3.1. Target structure

The point group symmetry of equilibrium Cl_2 is $D_{\infty v}$. Molecular symmetries can be taken advantage of to calculate the integrals between Gaussian-type orbital (GTO) basis functions, however, the Sweden-Molecule quantum chemistry codes [20], upon which the polyatomic UKRmol inner region codes used in this work are based, are limited to only using Abelian or commutative point groups. This is also true of MOLPRO [21], another quantum chemistry code which can be used to calculate the integrals between GTO basis functions used subsequently in the polyatomic UKRmol inner region codes. Due to this restriction, the non-Abelian symmetry $D_{\infty v}$ is represented in the D_{2h} point group.

The Cl_2 target was represented using a Dunning cc-pVTZ GTO basis set. The ground state of Cl_2, X $^1\Sigma_g^+$, has the configuration $[1\text{-}5\sigma_g, 1\text{-}2\pi_u, 1\text{-}4\sigma_u, 1\text{-}2\pi_g]^{34}$. **MOLPRO** was used to calculate these orbitals. The target was represented using a CAS-CI treatment, freezing electrons of the lowest 13 orbitals with 8 electrons from the 2 π HOMOS active in these open orbitals and 5 valence orbitals: $[1\text{-}5\ \sigma_g, 1\ \pi_u, 1\text{-}4\ \sigma_u, 1\ \pi_g]^{26}$

Table 1. Cl_2 equilibrium geometry.

	X (Å)	Y (Å)	Z (Å)
Cl	0.0	0.0	0.9940
Cl	0.0	0.0	−0.9940

Table 2. Comparison of vertical excitation energies for excited states of Cl_2 calculated in this work with those calculated by Rescigno [10], and Peyerimhoff and Buenker [23]. Energies are given for excited states up to and just above the measured IP of Cl_2 at 11.481 eV [24].

State	This work	[10]	[23]	State	This work	[23]
X $^1\Sigma_g^+$	0.000	0.00	0.00	C $^1\Delta_g$	7.790	8.12
a $^3\Pi_u$	3.252	3.36	3.31	D $^1\Sigma_g^+$	8.228	8.29
A $^1\Pi_u$	4.348	4.30	4.05	E $^1\Sigma_u^-$	8.982	9.43
b $^3\Pi_g$	6.498	6.38	6.29	d $^3\Delta_u$	9.113	
c $^3\Sigma_g^-$	7.257			e $^3\Sigma_u^+$	9.219	9.74
c′ $^3\Sigma_u^+$		7.02	6.87	f $^3\Sigma_u^-$	12.691	
B $^1\Pi_g$	7.537	7.01	6.83			

$[6\ \pi_g, 2\text{-}3\ \pi_u, 5\text{-}6\ \sigma_u, 2\text{-}3\ \pi_g]^8$. All calculations were performed at the Cl_2 equilibrium geometry sourced from the NIST Computational Chemistry Comparison and Benchmark Database [22] and given in table 1.

The vertical excitation energies (VEEs) of the excited states of Cl_2 calculated from this model are given in table 2 along with a comparison to published calculated values. The VEEs calculated in this work compare well to the published VEEs. Rescigno [10] and Peyerimhoff and Buenker [23] identified the fourth excited state of Cl_2 as B $^1\Pi_g$, whereas in this work we identified the fourth state as c $^3\Sigma_g^-$, and the B $^1\Pi_g$ state as the fifth excited state. The implications of the different symmetries of the c $^3\Sigma_g^-$ state identified in this work and the c′ $^3\Sigma_u^+$ state identified in [10, 23] for the calculated cross sections will be discussed in section 4.

The scattering calculation target used an **R**-matrix sphere of radius 10 a_0. The continuum basis was represented using GTOs with $\ell \leqslant 4$ (up to g orbitals) [25], which were orthogonalised to the target orbitals.

3.2. Dissociation of ground state Cl₂

The process of electron impact dissociation occurs when energy gained from the scattering electron promotes the molecule into an electronic state, which subsequently dissociates. This occurs when the dissociating bond is weakened by the transfer of electrons from bonding molecular orbitals, to orbitals away from the bonding region, which do not enforce the bond, and pull the nuclei apart. These orbitals are referred to as anti-bonding orbitals, orbitals that, if occupied, contribute to a reduction in the cohesion between the two atoms and raise the energy of the molecule above that of separated atoms [26].

As discussed by Peyerimhoff and Buenker [23], the σ_u orbital has anti-bonding character. As a result, excitation
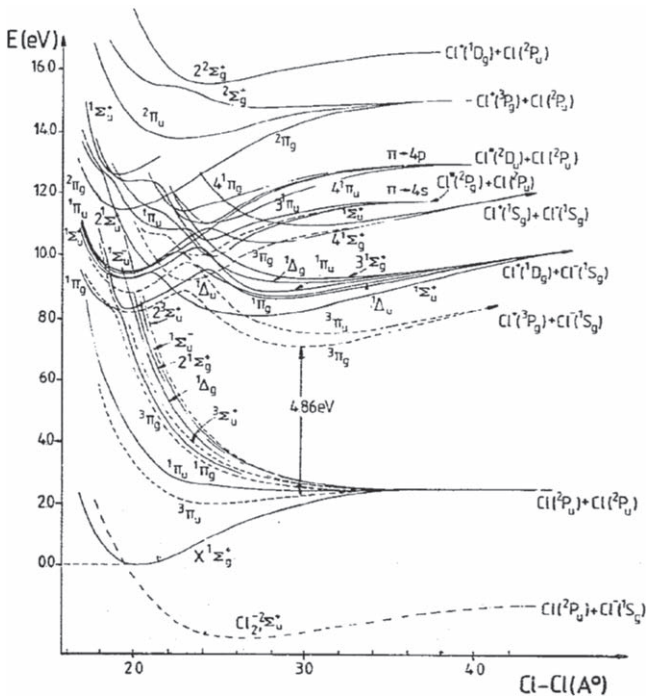
Figure 1. Composite potential energy diagram for Cl_2. Reproduced from Peyerimhoff and Buenker [23] under the terms of the Creative Commons Attribution-Non Commercial-No Derivatives License (CC BY-NC-ND).

processes that populate σ_u or σ_u^2 orbitals result in dissociation. Of the states listed in table 2, the following were found to fulfil this criteria by Peyerimhoff and Buenker [23] and dissociate to form two ground state Cl atoms: $a^3\Pi_u$, $A^1\Pi_u$, $b^3\Pi_g$, $c'^3\Sigma_u^+$, $B^1\Pi_g$, $C^1\Delta_g$, $D^1\Sigma_g^+$ and $e^3\Sigma_u^+$. The orbital movement for the $c^3\Sigma_g^-$ state identified in this work is assumed to be the same as that of the $c'^3\Sigma_u^+$ state identified in [23]. The $d^3\Delta_u$ and $f^3\Sigma_u^-$ states were not identified in the calculations of [23], as such, orbital movement information and potential energy curves are not available for these states. As a result, we cannot be certain of their dissociation pathway, so they are excluded from the remaining discussion on dissociation. In the work of [23] two $^1\Sigma_u^-$ states were identified; one dissociating to form two ground state Cl atoms, and the other a Rydberg state dissociating into one ground state Cl atom and Cl^+. Given that we cannot be certain which of the two states is identified in our calculations, we also exclude the $E^1\Sigma_u^-$ from further discussion on dissociation. The excluded states have significantly smaller cross sections than the lower lying states (at least 2–3 orders of magnitude lower than that of the $a^3\Pi_u$ state for all energies), therefore these exclusions have very little effect on the total dissociation cross sections presented later.

The nature of the excited states can be better understood through the Cl_2 potential energy curves shown in figure 1, taken from Peyerimhoff and Buenker [23], which also show the states of the Cl atoms produced by dissociation of the different excited states of Cl_2. All of the dissociative states considered in the results section of this work lead to the formation of two ground state Cl atoms.
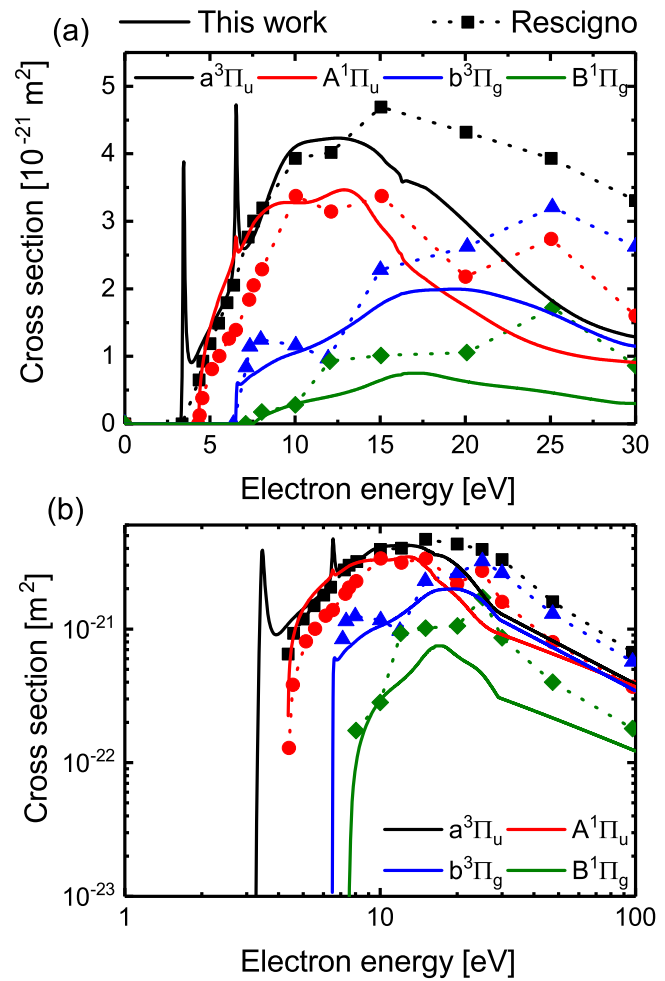

Figure 2. (a) Comparison between excitation cross sections from $Cl_2(X^1\Sigma_g^+)$ into dissociative Π states, with different spins and symmetries, calculated in this work and those calculated in [10] over the energy range originally calculated in [10] on a linear scale. (b) Comparison of the same data as shown in (a) on log axes to enable comparison over a wider energy range. Above 30 eV the scaling of the cross sections from [10] proposed by Grégorio and Pitchford [7], based on the experimental dissociation cross section of Cosby [12], is shown.

4. Results

4.1. Dissociation cross sections for Cl2

Figure 2 presents our calculated cross sections for excitation from ground state Cl_2 to the dissociative Π states (with various spins and symmetries), along with those calculated by Rescigno [10]. Figure 2(a) shows the data over the energy range originally calculated by Rescigno [10] on a linear scale. Figure 2(b) shows the data on log axes to enable comparison over a wider energy range. Above 30 eV the cross-sections from Rescigno [10] are scaled as proposed by Grégorio and Pitchford [7], based on the experimental dissociation cross section of Cosby [12]. The agreement between the cross sections from this work and those from Rescigno [10] is very good, particularly at energies up to around 15 eV. Our calculations show a few sharp peaks in the cross sections which can be associated with resonances. These features are too
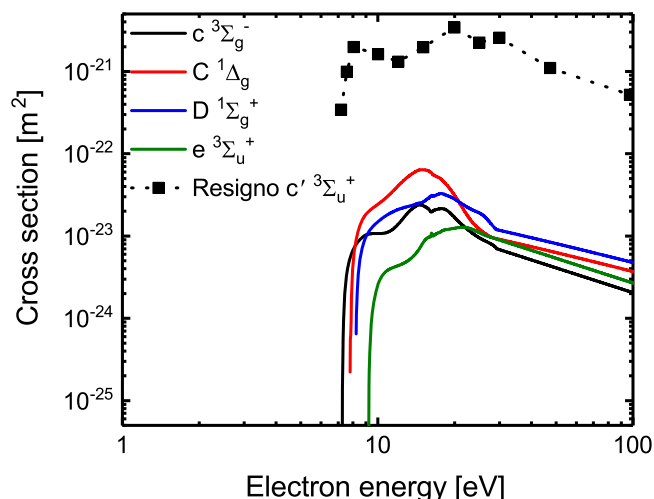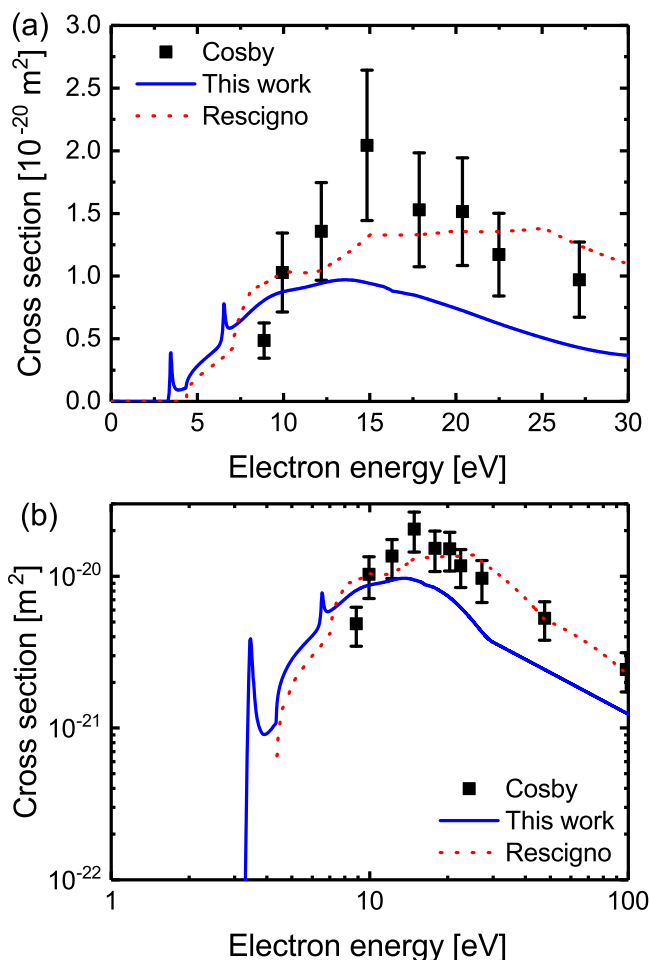
Figure 3. Calculated excitation cross sections from $Cl_2(X\ ^1\Sigma_g^+)$ into dissociative Δ and Σ states. The cross section to the $c'\ ^3\Sigma_u^+$ calculated in [10], but not identified in this work, is also shown. The scaling of this cross section above 30 eV is taken from Grégorio and Pitchford [7].

narrow to be resolved at the resolution of the experiments (shown in figure 4) or the calculations of Rescigno; however, the inclusion of vibrational motion, neglected in the present calculations, would be expected to broaden these resonance features. The precise role of these resonances in the electronic excitation of Cl_2 awaits further study.

Figure 3 shows the calculated cross sections for excitation into dissociative Δ and Σ states. The cross-section to the $c'\ ^3\Sigma_u^+$ state, calculated in [10] but not identified in this work, is also shown. Here, it is clear that the excitation cross-sections to the dissociative Δ and Σ states are much smaller in magnitude than the cross-sections to the Π states (shown in figure 2), but similar in shape. Furthermore, the cross-section for excitation of the $c'\ ^3\Sigma_u^+$ state calculated in [10] is significantly larger than (but similar in shape to) that of the $c^3\Sigma_g^-$ state identified in our work, despite their similar threshold energies. This is likely to be a result of the different symmetries of the states in the two calculations. According to Goddard *et al* [27] the electron scattering cross sections for $\Sigma_g^+ \leftrightarrow \Sigma_g^-$ transitions in a linear molecule must approach zero for scattering angles of 0° and 180°, since the reflection symmetry of the molecule ($+\leftrightarrow-$) cannot change during forward or backward collisions. In contrast, electron impact scattering cross sections for $\Sigma_g^+ \leftrightarrow \Sigma_u^+$ transitions, i.e. from the ground state to the $c'\ ^3\Sigma_u^+$ state as identified by Rescigno [10], are not constrained in this way, and therefore exhibit a larger integrated cross section.

Figure 4 shows a comparison of the sum of the excitation cross sections leading to dissociation calculated in this work, those calculated by Rescigno [10], and the measured dissociation cross section of Cosby [12]. As before, (a) shows the electron energy range originally calculated by Rescigno with linear axes, while (b) shows a comparison over a wider energy range with log axes. The summed dissociation cross section from Rescigno is larger above 15 eV and exhibits

Figure 4. (a) Comparison of total electron impact dissociation cross sections for $Cl_2(X\ ^1\Sigma_g^+)$ calculated in this work, those calculated in [10] and those measured by Cosby [12] on a linear scale over the energy range originally calculated in [10] on a linear scale. (b) Comparison of the same data as shown in (a) on log axes to enable comparison over a wider energy range. Above 30 eV the scaling of the cross sections from [10] proposed by Grégorio and Pitchford [7], based on the experimental dissociation cross section of Cosby [12], is shown.

better agreement with the measured total cross section of Cosby [12] in this range. However, it is important to emphasise that in the measurements of Cosby [12] the Cl_2 ground state target molecules were in a distribution of vibrational states due to the experimental technique used, whereas for the calculations in this work and Rescigno [10] only $Cl_2(v=0)$ was considered. As a result, the measurements and calculations are not directly comparable. Furthermore, calculations for electron-impact dissociation of vibrationally excited H_2, O_2 and N_2 molecules have shown that the magnitude of the dissociation cross section increases strongly as the vibrational level is increased [28–30]. As a result, we believe our calculations to be consistent with the data of Cosby, although further calculations of vibrational-state resolved electron-impact dissociation cross sections would be required to confirm this.

4.2. Rate coefficients for electron impact dissociation

In fluid and global plasma simulations, electron impact cross sections are typically incorporated in the form of rate coefficients, k, which are derived from the electron energy distribution function f through the relation:

$$k(T_{\mathrm{eff}}) = \left(\frac{2e}{m_e}\right)^{1/2} \int_0^\infty \sigma(\epsilon)\epsilon^{1/2} f(\epsilon)\, \mathrm{d}\epsilon. \qquad (2)$$

Here, T_{eff} is the effective electron temperature, e is the electron charge, m_e the electron mass and ϵ the electron energy. In low-temperature plasmas, the shape and effective temperature of the electron energy distribution function is highly variable, depending on parameters such as the nature of the plasma source, the operating pressure [31–33], the voltage/current [34, 35] the driving frequency [36–38] and the gas or gas mixture [39, 40]. The shape and temperature of the distribution function can also vary strongly in space and time within the same plasma source [41–46]. To understand how the cross sections calculated in this work affect the corresponding rate coefficients for electron impact dissociation we follow the approach of Gudmundsson [47] and Toneli *et al* [48] and define a general expression for the electron energy distribution function:

$$f(\epsilon) = c_1 \epsilon^{1/2} \exp(-c_2 \epsilon^x) \qquad (3)$$

The parameter x defines the shape of $f(\epsilon)$. $x = 1$ represents a Maxwellian distribution function, $x = 2$ resembles a Druyvesteyn distribution (similar to distribution functions found at higher gas pressures) and $x = 0.5$ gives a concave distribution function that is highly populated at low electron energies, while also having a pronounced high energy tail (similar to distribution functions found at low gas pressures). The parameters c_1 and c_2 are given by the expressions [47, 48]

$$c_1 = \frac{x}{\langle\epsilon\rangle^{3/2}} \frac{[\Gamma(\xi_2)]^{3/2}}{[\Gamma(\xi_1)]^{5/2}}, \qquad (4)$$

$$c_2 = \frac{1}{\langle\epsilon\rangle^x} \left[\frac{\Gamma(\xi_2)}{\Gamma(\xi_1)}\right]^x. \qquad (5)$$

Here, $\langle\epsilon\rangle$ is the mean electron energy $\langle\epsilon\rangle = 3/2 T_{\mathrm{eff}}$, Γ denotes a gamma function, $\xi_1 = 3/2x$ and $\xi_2 = 5/2x$.

Figure 5(a) shows the form of $f(\epsilon)$ for different values of x with $T_{\mathrm{eff}} = 3$ eV. Figure 5(b) shows a comparison between the dissociation rate coefficients derived from the total cross section calculated in this work and that calculated in [10] for varying T_{eff} and with $x = 0.5$, 1 and 2. As x is decreased from 2 to 0.5 the rate coefficient for dissociation increases for a given effective electron temperature because a greater proportion of electrons populate the part of the distribution function above the threshold energy for excitation of dissociative states. This is the case for both the cross sections calculated in this work and those calculated in [10]. For a given value of x the dissociation rate coefficients derived from the cross sections calculated in this work and those from [10] differ to varying degrees. These differences are greatest at low values of T_{eff} and when $x = 2$, under which conditions the
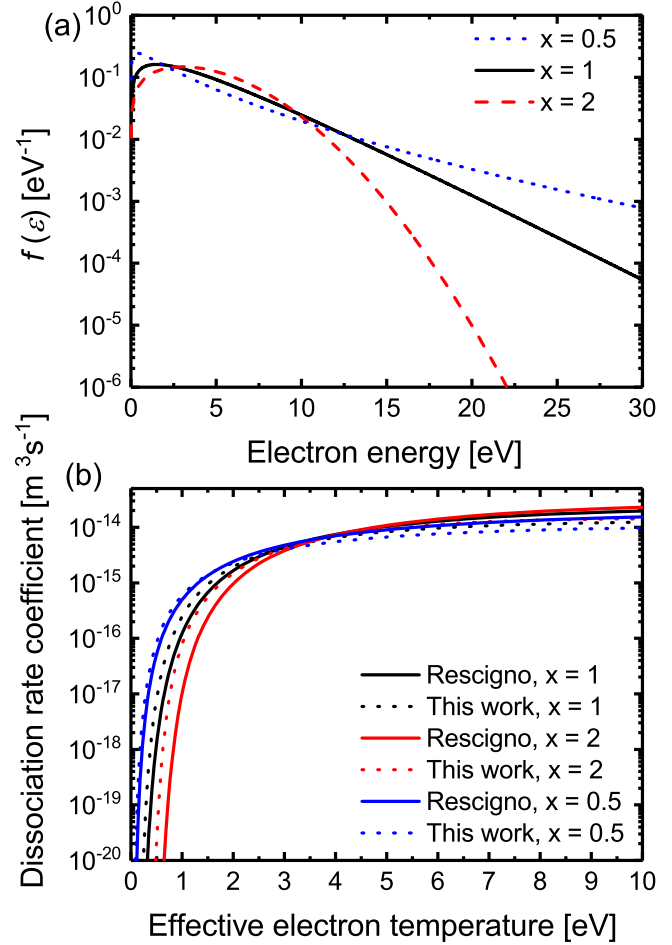
Figure 5. (a) Comparison of electron energy distribution functions $f(\epsilon)$ of different shapes (values of x) for the same effective electron temperature $T_{\mathrm{eff}} = 3$ eV. (b) Total electron impact dissociation rate coefficients calculated from the cross sections presented in this work, and those calculated by Rescigno [10], as a function of effective electron temperature T_{eff} for different shapes of $f(\epsilon)$ (values of x).

difference between the rate coefficients can be several orders of magnitude. This is also true (but to a lesser extent) when $x = 1$, but is significantly less important when $x = 0.5$. These differences have the potential to be important when modelling low T_{eff} plasmas, of interest for atomic layer etching and deposition, such as those produced by electron beams which have been shown to exhibit Maxwellian electron energy distribution functions with T_{eff} as low as 0.4 eV [49–51]. As T_{eff} increases to around 3 eV and above, the difference in rate coefficient becomes less pronounced, and therefore the impact of using the different dissociation cross section sets for modelling of plasmas will be less significant.

The differences in dissociation rate coefficients between the cross sections calculated in this work and those calculated in [10] in the low T_{eff} range are primarily a result of the higher energy resolution of our calculations around the excitation threshold, as shown in figures 2(b) and 4(b). These differences are particularly pronounced for the dominant dissociation cross section, i.e. that going via the a $^3\Pi_u$ state. Above $T_{\mathrm{eff}} = 3$ eV, the rate coefficients derived from the cross-sections calculated in this work are generally lower than those

from the cross sections calculated in [10]. This is a result of the lower magnitude of our cross sections at electron energies above 15 eV. The discrepancy in rate coefficients between the two cross section sets at higher T_{eff} reaches a maximum of a factor of 1.5 – 1.6 for all three values of x when $T_{\text{eff}} = 10$ eV. The strong differences between the rate coefficients for dissociation at low T_{eff} emphasises the importance of the near-threshold region of electron impact dissociation cross sections in low-temperature plasmas. This further emphasises the advantages of using theoretical calculations for the derivation of such cross sections, as they are capable of providing the required high resolution and are not limited by experimental detection limits.

5. Conclusions

In this work, electron impact dissociation cross sections for Cl_2 calculated using the UK molecular **R**-matrix code have been presented and discussed. The results are broadly consistent with the previous calculations of Rescigno [10] and the experimental measurements of Cosby [12]. The differences between the cross sections calculated in this work and those from [10] were most pronounced in the near-threshold region of the cross section for dissociation occurring through excitation of the a $^3\Pi_u$ state, and above 15 eV for all states for which cross sections have been calculated. The potential influence on plasma modelling of these differences was assessed through the calculation of electron impact dissociation rate coefficients for different electron energy distribution function shapes and effective temperatures. It is found that the most significant discrepancies in rate coefficients occur at low electron temperatures due to differences in the cross sections in the near-threshold region, whereas the differences in cross-sections above 15 eV were less significant. All cross sections presented in this work will be made freely available through the Quantemol database, QDB [52].

6. Data Management

Data underpinning the figures in this manuscript can be accessed at https://doi.org/10.15124/b11c65cf-2913-4c63-a522-2f57006cfb8a

Acknowledgments

ORCID iDs

Jonathan Tennyson https://orcid.org/0000-0002-4994-5238
Jean-Paul Booth https://orcid.org/0000-0002-0980-3278
Timo Gans https://orcid.org/0000-0003-1362-8000
Andrew R Gibson https://orcid.org/0000-0002-1082-4359

References

[1] Oehrlein G S, Metzler D and Li C 2015 *ECS J. Solid State Sci. Technol.* **4** N5041–53
[2] Kanarik K J, Lill T, Hudson E A, Sriraman S, Tan S, Marks J, Vahedi V and Gottscho R A 2015 *J. Vac Sci. Technol.* A **33** 020802
[3] Dorf L, Wang J C, Rauf S, Monroy G A, Zhang Y, Agarwal A, Kenney J, Ramaswamy K and Collins K 2017 *J. Phys. D: Appl. Phys.* **50** 274003
[4] Pitchford L *et al* 2013 *J. Phys. D: Appl. Phys.* **46** 334001
[5] Bartschat K and Kushner M J 2016 *Proc. Natl Acad. Sci. USA* **113** 7026–34
[6] Christophorou L G and Olthoff J K 1999 *J. Phys. Chem. Ref. Data* **28** 131–69
[7] Gregório J and Pitchford L 2012 *Plasma Sources Sci. Technol.* **21** 032002
[8] Ruf M, Barsotti S, Braun M, Hotop H and Fabrikant I 2004 *J. Phys. B: At. Mol. Opt. Phys.* **37** 41
[9] Kolorenč P and Horáček J 2006 *Phys. Rev.* A **74** 062703
[10] Rescigno T N 1994 *Phys. Rev.* A **50** 1382
[11] Cosby P C 1990 *Bull. Am. Phys. Soc.* **35** 1822
[12] Cosby P C and Helm H 1992 Dissociation rates of diatomic molecules *Technical Report* WL-TR-93-2004 Aero Propulsion and Power Directorate, Wright Laboratory
[13] Yadav H, Vinodkumar M, Limbachiya C and Vinodkumar P 2018 *J. Phys. B: At. Mol. Opt. Phys.* **51** 045201
[14] Burke P G 2011 *R-matrix Theory of Atomic Collisions (Springer Series on Atomic, Optical, and Plasma Physics)* (Berlin Heidelberg: Springer-Verlag)
[15] Carr J M, Galiatsatos P G, Gorfinkiel J D, Harvey A G, Lysaght M A, Madden D, Man Z, Plummer M, Tennyson J and Varambhia H N 2012 *Eur. Phys. J.* D **66** 58
[16] Tennyson J, Brown D B, Munro J J, Rozum I, Varambhia H N and Vinci N 2007 *J. Phys.: Conf. Ser.* **86** 012001
[17] Tennyson J 2010 *Phys. Rep.* **491** 29–76
[18] Tennyson J 1996 *J. Phys. B: At. Mol. Opt. Phys.* **29** 6185–201
[19] Hamilton J R, Tennyson J, Huang S and Kushner M J 2017 *Plasma Sources Sci. Technol.* **26** 065010
[20] Almlöf J and Taylor P R 1984 Computational Aspects of Direct SCF and MCSCF Methods *Advanced Theories and Computational Approaches to the Electronic Structure of Molecules (NATO ASI Series (Series C: Mathematical and Physical Sciences)* 133) ed C E Dykstra (Dordrecht: Springer)
[21] Werner H J *et al* 2012 *WIREs Comput. Mol. Sci.* **2** 242–53
[22] Johnson III R D 2018 NIST Computational Chemistry Comparison and Benchmark Database, NIST Standard Reference Database Number 101 Release 19 http://cccbdb.nist.gov/ (https://doi.org/10.18434/T47C7Z)

[23] Peyerimhoff S D and Buenker R J 1981 *Chem. Phys.* **57** 279–96

[24] Huber K P and Herzberg G 1979 *Molecular Spectra and Molecular Structure: IV. Constants of Diatomic Molecules* vol 716 (New York: Van Nostrand Reinhold)

[25] Faure A, Gorfinkiel J D, Morgan L A and Tennyson J 2002 *Comput. Phys. Commun.* **144** 224–41

[26] Atkins P and De Paula J 2010 *Atkin's Physical Chemistry Ninth Edition* 9th edn (Oxford: Oxford University Press)

[27] Goddard W III, Huestis D, Cartwright D and Trajmar S 1971 *Chem. Phys. Lett.* **11** 329–33

[28] Stibbe D T and Tennyson J 1998 *New. J. Phys.* **1** 2

[29] Laporta V, Little D, Celiberto R and Tennyson J 2014 *Plasma Sources Sci. Technol.* **23** 065002

[30] Laporta V, Celiberto R and Tennyson J 2015 *Phys. Rev. A* **91** 012701

[31] Godyak V A and Piejak R B 1990 *Phys. Rev. Lett.* **65** 996

[32] Lafleur T, Chabert P and Booth J P 2014 *Plasma Sources Sci. Technol.* **23** 035010

[33] Gudmundsson J and Ventéjou B 2015 *J. Appl. Phys.* **118** 153302

[34] Godyak V, Piejak R and Alexandrovich B 1992 *Plasma Sources Sci Technol.* **1** 36

[35] Huang S and Gudmundsson J 2014 *Plasma Sources Sci. Technol.* **23** 025015

[36] Godyak V, Piejak R and Alexandrovich B 2002 *Plasma Sources Sci. Technol.* **11** 525

[37] Kim H C and Lee J K 2004 *Phys. Rev. Lett.* **93** 085003

[38] Gudmundsson J T, Snorrason D I and Hannesdottir H 2018 *Plasma Sources Sci. Technol.* **27** 025009

[39] Logue M D and Kushner M J 2015 *J. Appl. Phys.* **117** 043301

[40] Fiebrandt M, Oberberg M and Awakowicz P 2017 *J. Appl. Phys.* **122** 013302

[41] Gans T, Schulz-Von D G V and Döbele H 2004 *Europhys. Lett.* **66** 232

[42] Schulze J, Gans T, O'Connell D, Czarnetzki U, Ellingboe A R and Turner M M 2007 *J. Phys. D: Appl. Phys.* **40** 7008

[43] Song S H and Kushner M J 2012 *Plasma Sources Sci. Technol.* **21** 055028

[44] Schüngel E, Brandt S, Donkó Z, Korolov I, Derzsi A and Schulze J 2015 *Plasma Sources Sci. Technol.* **24** 044009

[45] Hurlbatt A, Gibson A R, Schröter S, Bredin J, Foote A P S, Grondein P, O'Connell D and Gans T 2017 *Plasma Process. Polym.* **14** 1600138

[46] Tsutsumi T, Greb A, Gibson A R, Hori M, O'Connell D and Gans T 2017 *J. Appl. Phys.* **121** 143301

[47] Gudmundsson J 2001 *Plasma Sources Sci. Technol.* **10** 76

[48] Toneli D A, Pessoa R S, Roberto M and Gudmundsson J T 2015 *J. Phys. D: Appl. Phys.* **48** 495203

[49] Lock E, Fernsler R and Walton S 2008 *Plasma Sources Sci. Technol.* **17** 025009

[50] Boris D, Petrov G, Lock E, Petrova T B, Fernsler R and Walton S 2013 *Plasma Sources Sci. Technol.* **22** 065004

[51] Rauf S, Balakrishna A, Agarwal A, Dorf L, Collins K, Boris D R and Walton S G 2017 *Plasma Sources Sci. Technol.* **26** 065006

[52] Tennyson J *et al* 2017 *Plasma Sources Sci. Technol.* **26** 055014